sciendo

Effects of Al doping on defect behaviors of ZnO thin film as a photocatalyst

FUCHENG YU*, HAILONG HU, BOLONG WANG, HAISHAN LI, TIANYUN SONG, BOYU XU,
LING HE, SHU WANG, HONGYAN DUAN

School of Material Science and Engineering, School of Mechanical and Electrical Engineering, Lanzhou University of
Technology, Lanzhou 730050, P. R. China

Al doped ZnO (AZO) thin films were prepared on silica substrates by sol-gel method. The films showed a hexagonal wurtzite structure with a preferred orientation along c-axis. Suitable Al doping dramatically improved the crystal quality compared to the undoped ZnO films. Dependent on the Al dopant concentration, the diffraction peak of (0 0 2) plane in XRD spectra showed at first right-shifting and then left-shifting, which was attributed to the change in defect concentration induced by the Al dopant. Photocatalytic properties of the AZO film were characterized by degradation of methyl orange (MO) under simulated solar light. The transmittance of the films was enhanced by the Al doping, and the maximum transmittance of 80 % in the visible region was observed in the sample with Al concentration of 1.5 at.% (mole fraction). The film with 1.5 at.% Al doping achieved also maximum photocatalytic activity of 68.6 % under solar light. The changes in the film parameters can be attributed to the variation in defect concentration induced by different Al doping content.

Keywords: *sol-gel; ZnO thin film; Al doping; photocatalyst*

1. Introduction

ZnO is a transparent direct wide-band gap II-VI compound semiconductor with a bandgap of 3.37 eV and exciton binding energy of 60 meV at room temperature, which makes it an efficient exciton emission material at room temperature [1, 2]. The band gap engineering of ZnO is essential for developing transparent photonic devices, transparent electronic devices and transparent conductive electrodes. Due to the excellent properties, ZnO is furthermore considered as a very promising functional material for electronics, optoelectronics, nanoelectronics and electronic devices, such as ultraviolet-visible (U-Vis) lasers, light-emitting diodes, field emission devices, high-performance sensors, solar cells, piezoelectric nanogenerators [3–6].

Moreover, ZnO is an attractive material in photocatalytic field due to its unique properties [7]. However, two shortages affect the application of ZnO as a photocatalyst: (1) the wide band gap

limits its application to the ultraviolet region, and (2) the high recombination rate of exitons shortens the exciton lifetime. The UV radiation accounts for only 4 % of the incoming solar radiation, while about 43 % of solar energy belongs to the visible light (wavelength between 390 nm to 760 nm). Thus, many researchers attempt to expand the photoresponse of ZnO to visible light region [8, 9]. In the studies, doping with the elements such as Al, In, Ga, is a typical method to improve the properties of ZnO. Among the dopants, Al has proven to be effective to obtain high quality samples with the modified transparency and emission efficiency in the visible and ultraviolet/blue regions [10–13]. Many studies showed that the Al doped ZnO (AZO) thin film can improve the electric properties effectively compared with undoped ZnO thin film [14]. Furthermore, AZO thin film has many other advantages, such as rich resources, low price, non-toxicity, excellent stability, etc. Many methods have been adopted for the preparation of AZO film, including sol-gel, chemical vapor deposition, molecular beam epitaxy (MBE), magnetron sputtering [15–19], etc. Different techniques

---

for the preparation of ZnO film have given ZnO thin film with slightly differentiated properties. Among these techniques, sol-gel process has distinct advantages over other approaches, such as the simple process, uniform film quality, and low cost [20].

The structural and optical properties of doped ZnO thin film is also a valuable topic for the study of ZnO thin films. In this paper, the effects of Al doping on the structural and optical properties of ZnO thin film have been studied to reveal the relationship between crystal structure, defects and optical properties. Furthermore, the photocatalytic behavior of AZO film in the degradation of MO solution have been investigated.

2. Experimental

The AZO samples were synthesized by sol-gel method on silica substrates. Zinc acetate dihydrate [$Zn(CH_3COO)_2 \cdot 2H_2O$, purity $\geqslant$ 99.99 %] was selected as the precursor, and aluminum nitrate nonahydrate ($Al(NO_3)_3 \cdot 9H_2O$) was adopted as a source material of Al dopant. A certain amount of $Zn(CH_3COO)_2 \cdot 2H_2O$ was dissolved in the mixed solution of ethanol and monoethanolamine ($HO(CH_2)_2NH_2$, (MEA), purity $\geqslant$ 99.0 %), and the solution was stirred at room temperature for 30 minutes, then a certain amount of $Al(NO_3)_3 \cdot 9H_2O$ was added. The final solution was stirred at 70 °for 2 hours, and the homogeneous sol solution was obtained. Then the solution was left for 48 hours to stabilize. The molar ratio of MEA to $Zn(CH_3COO)_2 \cdot 2H_2O$ was kept constant at 1:1, where the concentration of $Zn(CH_3COO)_2$ was fixed at 0.6 mol/L, while the Al molar concentration varied from 0 at.% to 2.0 at.%.

The AZO samples were prepared by repeated spin-coating with a rotational speed of 3000 rpm to get an expected thickness. Before the deposition, the silica substrates were ultrasonically cleaned in distilled water, hydrochloric acid, acetone, and ethanol in turn. The samples were preheated at 400 °C for 1 hour after each gel layer coating, which was repeated several times as required. Finally, the samples were annealed at 900 °C for 1 hour, and a layer of AZO thin film
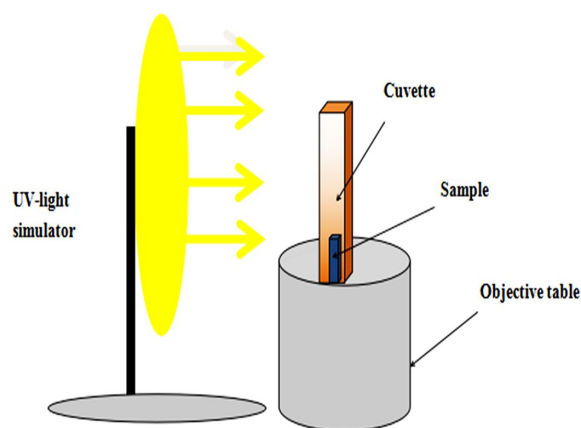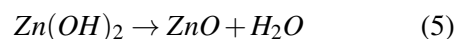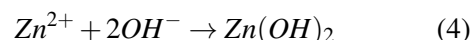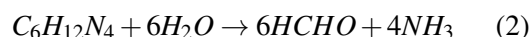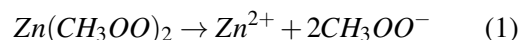

Fig. 1. Schematic diagram of the photocatalysis system.

on the silica substrate with a thickness about 500 nm was formed. The final volume of the ZnO film was 10 mm × 10 mm × 500 nm.

The formation mechanism of ZnO is as follows [21]:

$$Zn(CH_3OO)_2 \rightarrow Zn^{2+} + 2CH_3OO^- \qquad (1)$$

$$C_6H_{12}N_4 + 6H_2O \rightarrow 6HCHO + 4NH_3 \qquad (2)$$

$$NH_3 + H_2O \rightarrow NH_4^+ + OH^- \qquad (3)$$

$$Zn^{2+} + 2OH^- \rightarrow Zn(OH)_2 \qquad (4)$$

$$Zn(OH)_2 \rightarrow ZnO + H_2O \qquad (5)$$

To investigate the photocatalytic characteristics of the AZO samples, 5 mL (0.02 mol/L) MO ($C_{14}H_{14}N_3O_3S\cdot Na$, AR) solution was prepared. The AZO samples were dipped in the solution, and the solution concentration was checked every 30 minutes under irradiation of simulated solar light. The power, current and voltage of the Xe lamp (CEL-500/350) were 500 W, 20 A and 20 V, respectively, and the distance between the Xe lamp and the MO solution was about 15 cm. The change in MO solution concentration during the photocatalytic degradation was measured by a UV-Vis spectrometer.

Fig. 1 shows a schematic diagram for the study of photocatalytic activity of ZnO as a catalyst under irradiation with simulated solar light.

The surface morphologies of the AZO samples were characterized by a field emission scanning electron microscopy (FE-SEM), the structural properties of the samples were investigated by an X-ray diffractometer (XRD), and the optical properties were examined by UV-Vis spectroscopy and photoluminescence (PL).

3.   Results and discussion

The X-ray patterns presented in Fig. 2 confirm the wurtzite structure of the AZO samples. Fig. 2a describes the XRD patterns of ZnO films prepared at different rotational speeds of spin-coating during the sample preparation process. The characteristic peaks indicate that the ZnO sample fabricated at a low rotation speed of 60 rpm has a wurtzite structure. When the rotational speed was increased to 3000 rpm, only the (0 0 2) peak became distinct while other peaks became fuzzy, which illustrates a preferred orientation along the (0 0 2) plane of the lattice at $2\theta = 34.43°$. The X-ray diffraction patterns in Fig. 2b belong to the samples fabricated at 3000 rpm and show a preferred orientation of hexagonal wurtzite structure. As shown in Fig. 2b, the peak intensity of the XRD patterns increases firstly, and then decreases, depending on Al doping concentrations. The strongest (0 0 2) peak appears in the AZO sample with Al concentration of 1.5 at.%. Fig. 2c shows an enlarged image of Fig. 2b, where a peak shifting can be observed obviously. With increasing of Al content, right-shifting of the peak followed by left-shifting can be observed. This is caused by the difference in the ions radii of Al^{3+} (0.54 Å), and Zn^{2+} (0.74 Å) [22]. At a low Al concentration, Al ions mainly occupy substitutional positions of Zn ions more than other positions in the lattice, which causes a shrinkage of the crystal, thereby a reduction of lattice parameter which leads to a right-shifting of the (0 0 2) peak in X-ray measurement. While at a high Al concentration, exceeding 0.5 at.%, the Al amount exceeds the solid solubility limit in ZnO crystal, the excessive dopant atoms go into the interstitial

space of ZnO lattice which induces an expansion of ZnO lattice. When the doping concentration of Al approaches 2 at.%, a slight right-shifting appears on the (0 0 2) peak which indicates a shrinkage of the lattice. The heavy doping leads to the formation of Al related second phase existing at grain boundaries which stresses the lattice and results in the lattice shrinkage. The amount of the second phase is too low to be detected with X-ray measurement, however, it is confirmed with the following SEM measurement. Therefore, at the Al doping concentration of 1.5 at.%, the distortion of lattice is compensated by the substituted Al ions and the interstitial Al atoms. Fig. 2d shows the relationship between the full width at half maximum (FWHM) and the grain size. With the increase of doping concentration, the FWHM decreases at first and then increases, while the internal stress increases at first and then decreases, which is caused by the doping of Al ions as discussed above, coinciding with the opinion of other researchers [21]. Grain size is usually calculated by Scherer equation [23]:

$$D = K\lambda/(\beta \cos\theta) \qquad (6)$$

D is the grain size, K is a constant, λ is the wavelength, β is FWHM, θ is diffraction angle. The calculated grain sizes of the AZO samples varied from 30 nm to 50 nm.

Linear refractive index can be obtained through the following equation [24]:

$$N = \alpha + \beta E_g \qquad (7)$$

N is the linear refractive index, α is absorption coefficient ($\alpha = 4.048$), β is FWHM, E_g is a band gap energy. The calculated linear refractive indexes for undoped ZnO and 1.5 at.% Al doped ZnO samples are 4.65497 and 4.61905 [25].

The surface morphologies of the ZnO film samples with different Al concentrations are presented in Fig. 3. As shown in Fig. 3, with increasing of Al concentration, the crystal quality of the AZO film becomes better which is confirmed by the increase in grain size, the decrease of surface defects, as well as uniformity of the grains. It shows that a proper amount of Al doping can improve the crystal quality of ZnO sample. In contrast, the excess Al
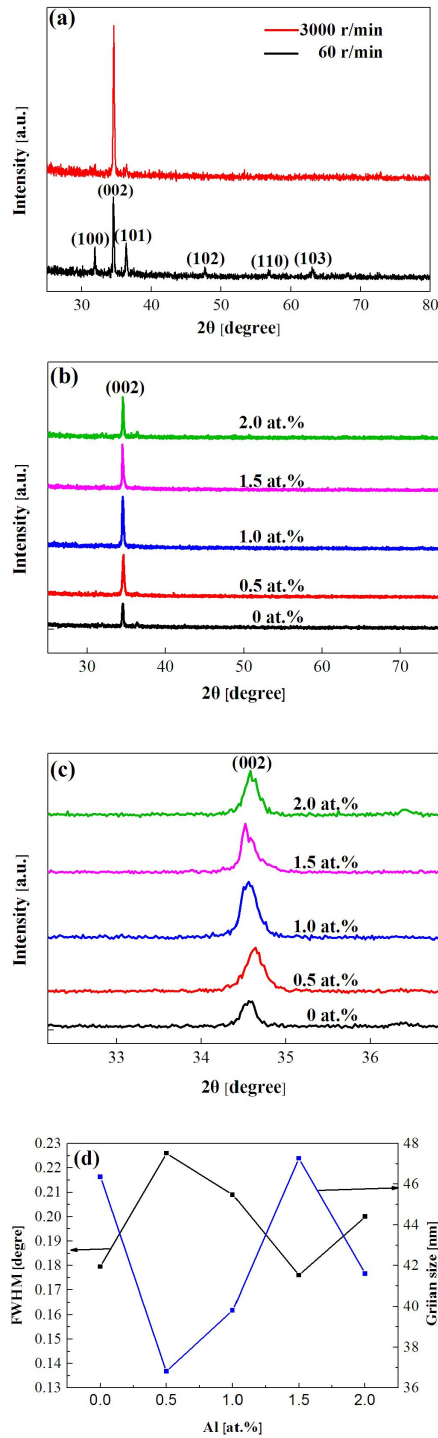
Fig. 2. X-ray measurements: (a) XRD patterns of ZnO films prepared at the different rotational speeds; (b) XRD patterns of the AZO samples with different Al content; (c) enlarged image of (b), and (d) relationship between the FWHM and the grain size.
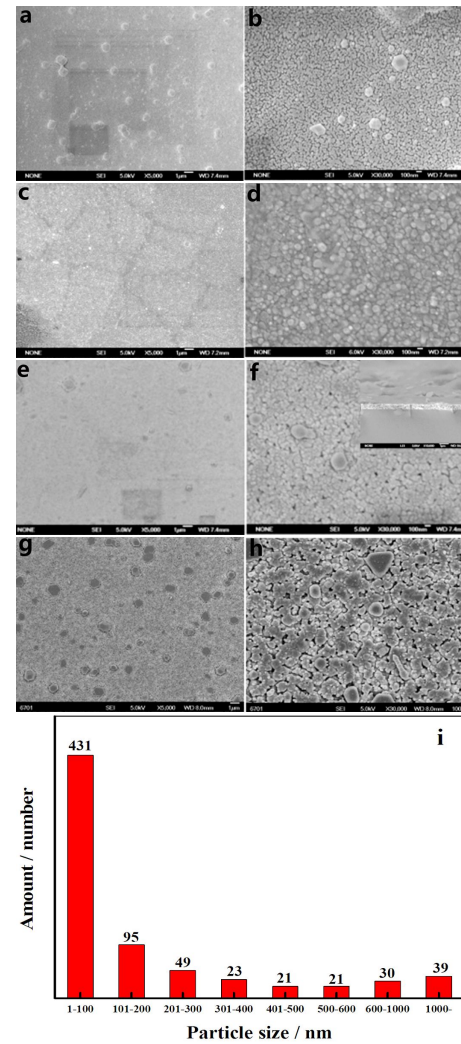

Fig. 3. SEM images of AZO samples with different Al content of 0.5 at.% (a, b), 1.0 at.% (c, d), 1.5 at.% (e, f), and 2.0 at.% (g, h); (i) distribution of grain sizes on the surface of a sample doped with 1.5 at.% Al.
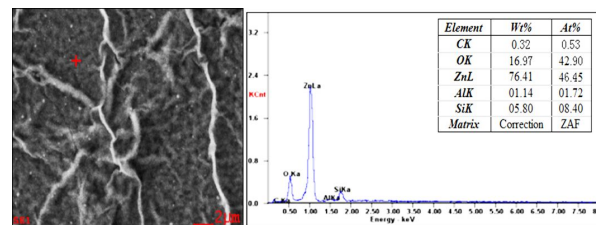

Fig. 4. Energy dispersive X-ray spectrum (EDXS) of an AZO sample doped with 1.5 at.% Al.

doping leads to a loose morphology of the sample, as shown in Fig. 3g and Fig. 3h, due to the formation of Al related second phase at the grain boundaries which can be easily observed as numerous white dots in Fig. 3h. The results are well consistent with the X-ray measurement. The grain sizes of the sample doped with 1.5 at.% Al were examined by the SEM at a magnification of ×30000, as shown in Fig. 3i. Particles with the size in 1 nm to 200 nm range cover 76.2 % of all particles. Fig. 4 shows an energy dispersive X-ray spectrum (EDXS) for the 1.5 at.% of Al doped ZnO sample. The atomic ratio of O, Zn and Al is 42.90:46.45:1.72, which indicates that Zn atoms are slightly in excess in the sample due to escape of O atoms from the crystal during the heat treatment process. The escape of O atoms also brings an amount of O vacancies which are favorable for utilization of visible light.

UV-Vis absorption spectra of the AZO samples are shown in Fig. 5a, where the absorption peak at 385 nm is an intrinsic peak of ZnO attributed to the Al related defect energy level in ZnO lattice. The peak intensity shows a decreasing tendency with increasing Al content [26]. In the sample doped with 2.0 at.% Al, as discussed in X-ray measurement, the formation of Al related precipitates at grain boundaries stresses the ZnO lattice what leads to the reduction of intrinsic peak intensity. Furthermore, with the increasing Al concentration, the absorption edge shifts towards the high energy region, which can be explained by the Burstein-Moss effect. The substitution of Al^{3+} ions for Zn^{2+} ions induces a shift of Fermi level towards the conduction band in ZnO crystal which results in a slight increase of band-gap. Fig. 5b shows the transmission spectra for all AZO and undoped ZnO samples, where the maximum transmittance of 80 % in visible light region is observed in the sample with 1.5 at.% Al doping. Depending on Al doping concentration, the transmittance of the samples increases firstly and then decreases in the visible region which corresponds to the change in the crystal quality due to the introduction of the dopant. The optical band gap was evaluated from the plot of $(\alpha h\nu)^2$ versus $h\nu$, by extrapolating the vertical straight line to the intercept with energy axis as shown in Fig. 5c. The following equation was adopted for the calculation [27]:

$$(\alpha h\nu)^2 = B(h\nu - E_g), \qquad (8)$$

where $h\nu$ is photon energy, B is a constant, E_g is optical band gap, and α is absorption coefficient. The α is absorption coefficient obtained from the following equation:

$$\alpha = (1/t)\ln T \qquad (9)$$

where T is transmittance and t is film thickness.

As shown in the plot in Fig. 5c, the Al content dependent optical band gap energy E_g varies from 3.232 eV to 3.256 eV. The maximum optical band gap of 3.256 eV was obtained for the sample with 1.5 at.% Al doping which is attributed to the growth of grain size due to Al doping in ZnO lattice. The result is consistent with the XRD measurements and SEM results.

Table 1. Band gap energies of different AZO samples.

Al [at.%]	E_g [eV]
0	3.232
0.5	3.249
1.0	3.250
1.5	3.256
2.0	3.253

Photoluminescence (PL) measurements of the AZO samples are displayed in Fig. 6a. A strong light emission near 395 nm existing in all the samples is attributed to the free exciton recombination [27]. The two peaks of blue light emission at about 420 nm and 430 nm are induced by interstitial oxygen defects (O_i) and interstitial zinc defects (Zn_i), respectively [28]. In addition, two sharp peaks at about 465 nm and 510 nm corresponding to cyan and green emission regions, respectively, which are induced by oxygen vacancy defects, are clearly visible for all the samples. Generally, there are three types of oxygen vacancies in ZnO crystal: V_o^{++} having two positive charges without capturing any electrons, V_o^+ having one positive charge with capturing of one electron, and neutral V_o^o with capturing of two electrons [29].
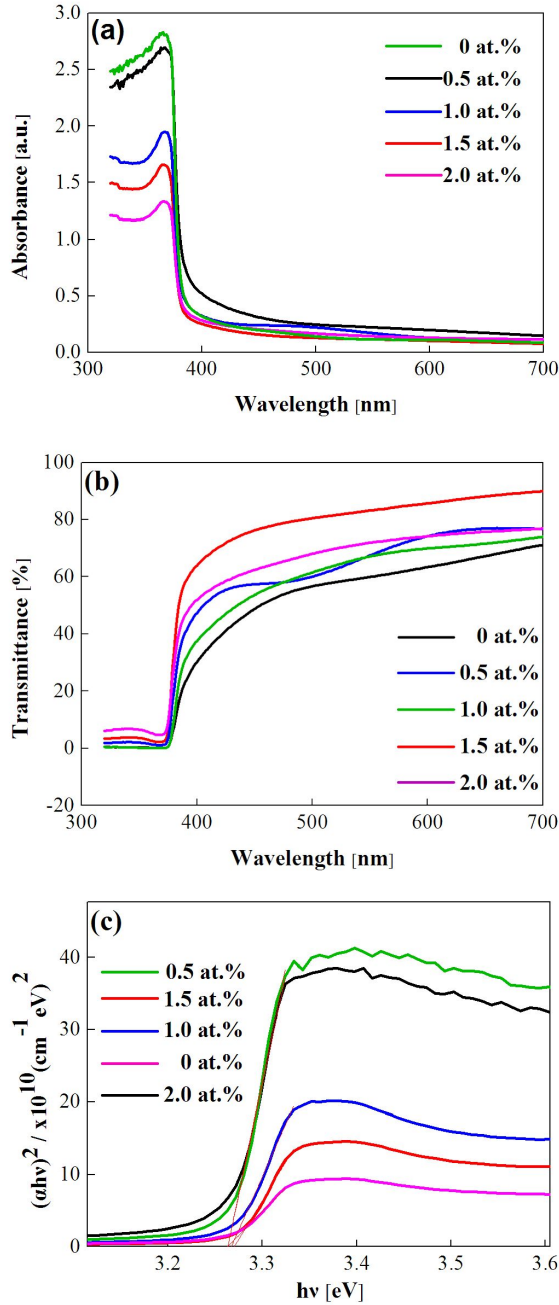
Fig. 5. UV-Vis spectra of AZO samples, (a) comparison of absorption spectra of the AZO samples, (b) comparison of transmission spectra of the AZO samples, and (c) plots of $(\alpha h\nu)^2$ versus $h\nu$.

Fig. 6. (a) PL spectra of AZO samples, (b) scheme of light emission mechanism.

The defect energy levels in AZO energy band are shown in Fig. 6b [30, 31] where the cyan light emission around 465 nm is connec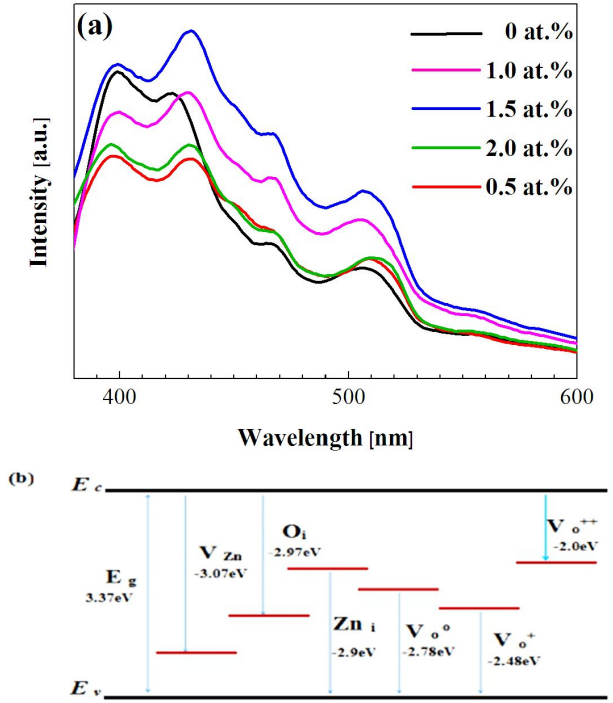ted with electron transition from the neutral oxygen vacancy (V_O^o) to the valence band, and the green light around 510 nm is related to electron transition from the V_O^+ to the valence band. The light emission corresponding to electron transition from the conduction band to the V_O^{++} is about 620 nm which is out of the measurement range.

The intensities of the peaks at about 465 nm and 510 nm for AZO samples are obviously higher than for undoped ZnO film, which is caused by the electronegativity difference between Zn^{2+} ion and Al^{3+} ion, where the electronegativity of the Al^{3+} ion and Zn^{2+} ion is 1.61 and 1.65, respectively. The binding energy of Al^{3+} ion and O^{2-} ion is weaker than that of Zn^{2+} ion and O^{2-} ion in ZnO lattice which leads to an increase in oxygen vacancy concentration during the heat treatment process. The intensity of these two peaks increases firstly, and then decreases, with Al doping concentration in the investigated range what reveals the oxygen vacancy concentration in ZnO lattice is dependent on Al doping. At high Al doping of 2.0 at.%, the supersaturated solid solution state is broken which causes a reduction of Al amount in the crystal,
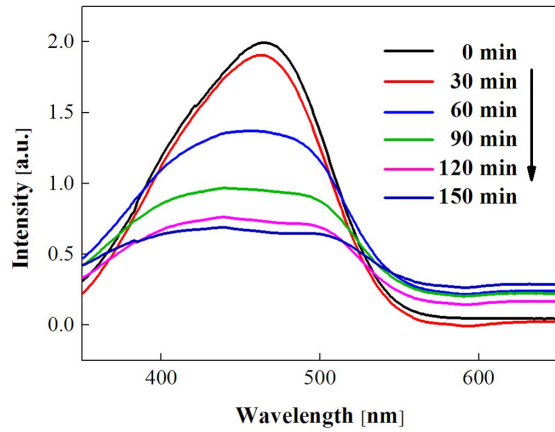
Fig. 7. Time dependence of MO concentration photo-catalyzed by 1.5 at.% of Al doping ZnO samples.

Fig. 8. Sketch of MO degradation efficiency with time for ZnO and different Al concentrations in AZO samples.

moving of the excessive Al atoms to the grain boundaries and forming Al related second phase separated from the AZO crystal.

The photocatalytic activity of the AZO sample with Al content of 1.5 at.% was evaluated by photocatalytic degradation of MO solution. The time dependence of MO concentrations for the sample is shown in Fig. 7. The intensity of the characteristic absorption peak of MO solution at the wavelength of 465 nm demonstrates a time dependent decrease (from 0 min to 150 min) which indicates degradation of MO solution.

The photocatalytic activities of undoped ZnO and AZO samples for MO solution are shown in Fig. 8. The photocatalytic rate of the samples is accelerated with increasing of Al doping from 0 at.% to 1.5 at.%, and the highest photocatalytic efficiency is observed in the sample with 1.5 at.% Al doping. Further increase in Al concentration, above 1.5 at.% results in a decrease in the photocatalytic efficiency. The excessive doping leads to crystal quality degradation, as well as a decrease in oxygen vacancy concentration, which is favorable to the recombination of electrons and holes in the AZO crystal and results in a reduction of hole and electron concentrations.

The following formula was used for the calculation of photocatalytic efficiency [32, 33]:

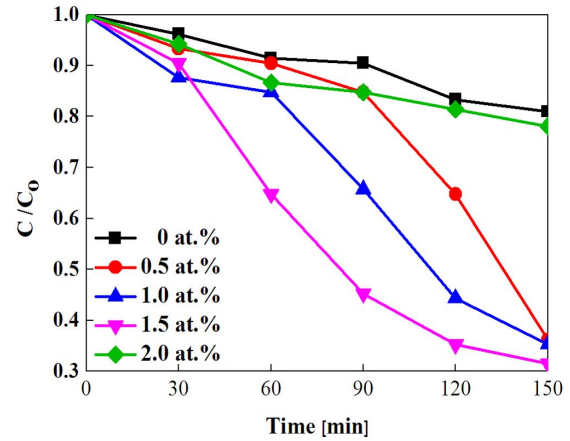$$\eta = (C_o - C)/C_o) \times 100\%, \qquad (10)$$

where, η is the photocatalytic efficiency, C_o is the initial concentration of MO, and C is the actual concentration of the MO solution. The optimum photocatalytic efficiency of about 68.6 % was obtained for the 1.5 at.% of Al doped ZnO sample after 150 minutes photocatalytic action.
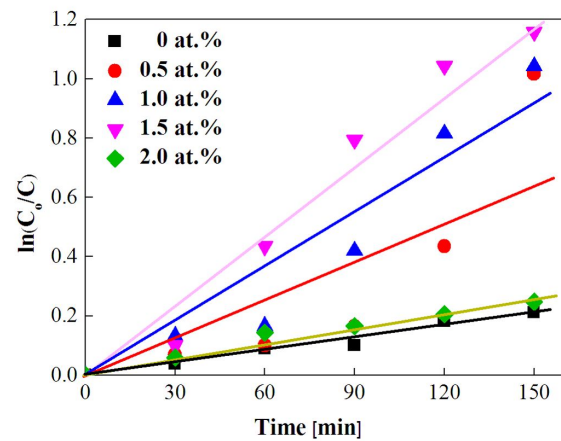

Fig. 9. Sketch of MO degradation vs. time under visible light irradiation.

A plot of time dependent $\ln(C_o/C)$ for the photodegradation behavior of MO is shown in Fig. 9. The relationship obeys pseudo-first-order kinetics [34, 35].

$$\ln(C_o/C) = kt \qquad (11)$$

where C_0/C is the normalized MO concentration, t is the reaction time, and k is the reaction rate constant.

The degradation rate constants k of MO solution under the presence of ZnO and AZO samples are given in Table 2. The highest degradation rate of $7.9 \times 10^{-3} \cdot min^{-1}$ was achieved for the sample with 1.5 at.% Al doping.

Table 2. Degradation rate constants of MO solution in the presence of AZO samples.

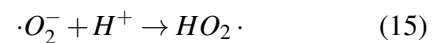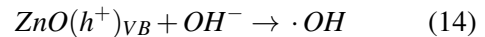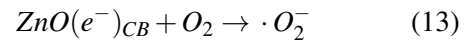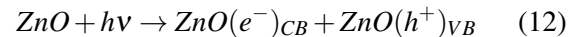| Sample	k $[min^{-1}]$
Undoped-ZnO	1.3×10^{-3}
Al (0.5 at.%)-doped ZnO	4.1×10^{-3}
Al (1.0 at.%)-doped ZnO	6.5×10^{-3}
Al (1.5 at.%)-doped ZnO	7.9×10^{-3}
Al (2.0 at.%)-doped ZnO	1.4×10^{-3}
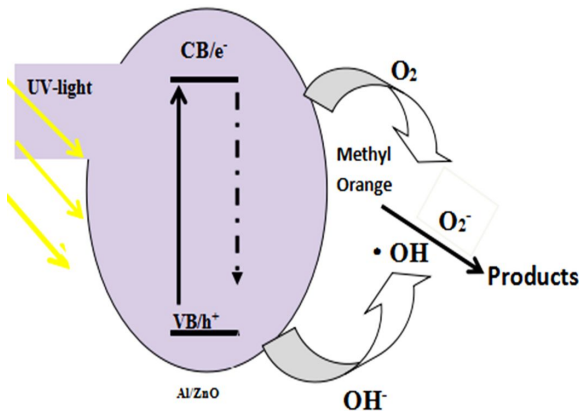
Fig. 10. Schematic illustration of the photocatalytic mechanism for organic pollutants degenerated by ZnO catalyst.

In Fig. 10, the photocatalytic mechanism of undoped ZnO and AZO samples is illustrated. When a ZnO semiconductor is irradiated by photons with energy no less than its energy band gap, the electrons are excited from the valence band to the conduction band, leaving holes in the valence band. However, in case of the relative wide band gap semiconductor, such as ZnO, the excited electrons would drop rapidly to the dopant energy levels, or to the valence band and recombine with the holes,

which is accompanied by emitting light of different wavelengths. The Al doping not only increases the number of electrons transported to the conduction band, but also inhibits the recombination rate of the electrons and holes in the valence band. Al doping leads to an increase in oxygen vacancy concentration (V_o^+ and V_o^{++}) in the forbidden band, and the electrons dropping from the conduction band are partly captured by the oxygen vacancies, thereby the amount of electrons reaching the valence band is significantly reduced which makes a lot of holes reserved in the valence band. The Al content dependent oxygen vacancy concentration coincides with the XRD and PL measurement results. The holes interact with water molecules or hydroxyls absorbed on the sample surface and the reactive hydroxyl radicals are created. The electrons act on the O_2 adsorbed on the semiconductor surface and form reactive superoxide radicals. These radicals react with organic dyes and produce CO_2 and H_2O, so as to achieve photocatalysis [36]. The reaction processes can be understood with the following chemical equations [34–37]:

$$ZnO + h\nu \rightarrow ZnO(e^-)_{CB} + ZnO(h^+)_{VB} \quad (12)$$

$$ZnO(e^-)_{CB} + O_2 \rightarrow \cdot O_2^- \quad (13)$$

$$ZnO(h^+)_{VB} + OH^- \rightarrow \cdot OH \quad (14)$$

$$\cdot O_2^- + H^+ \rightarrow HO_2 \cdot \quad (15)$$

$$HO_2 \cdot \rightarrow O_2 + H_2O_2 \quad (16)$$

$$H_2O_2 + \cdot O_2^- \rightarrow \cdot OH + OH^- + O_2 \quad (17)$$

$$\cdot OH + Dye(MO) \rightarrow products \quad (18)$$
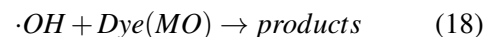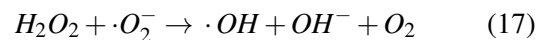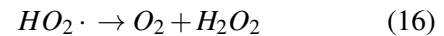
4. Conclusions

AZO samples with satisfying optical performance have been fabricated by sol-gel method. The transmittance of the samples in visible light region first increases with increasing Al content, reaches a maximum of 80 % for the sample with 1.5 at.% Al fraction, and then decreases. The photocatalytic activity of AZO samples is well corresponding to the transmittance of the samples, and the maximum photocatalytic activity of 68.6 % under the simulated solar light is also observed in the sample with 1.5 at.% Al doping. The doping of Al increases the defect (Zn_i, V_o^o and V_o^+) concentration which provides more electrons to the conduction band of ZnO crystal. Furthermore, the defect levels inhibit direct jumping of electrons from the conduction band to the valence band, and increase the numbers of effective holes and electrons, thereby the photocatalytic efficiency is improved greatly.

References

[1] PEARTON S.J., NORTON D.P., IP K., HEO Y.W., STEINER T., *J. Prog. Mater. Sci.*, 50 (2005), 293.

[2] KUMAR N., SRIVASTAVA A., *J. Alloy. Compd.*, 735 (2018), 312.

[3] BACHTOLD A., HADLEY P., NAKANISHI T., DEKKER C., *J. Sci.*, 294 (2001), 435.

[4] KAMARUDDIN S.A., CHAN K.-Y., YOW H.-K., SAHDAN M.Z., SAIM H., KNIPP D., *J. Appl. Phys. A-Mater.*, 104 (2011), 263.

[5] WEI A., SUN X.W., *J. Appl. Phys. Lett*, 88 (2006), 215.

[6] LING H., YUHUA W., WEIMIN S., *J. Rare Earth*, 27 (2009), 385.

[7] AMETA R., AMETA S.C., *CRC Press*, 2016.

[8] KLINGSHIRN C., *Phys. Status Solidi B*, 244 (2007), 3027.

[9] REIMER T., PAULOWICZ I., RÖDER R., KAPS S., LUPAN O., CHEMNITZ S., BENECKE W., RONNING C., ADELUNG R., MISHRA Y.K., *ACS Appl. Mater. Interfaces*, 6 (2014), 7806.

[10] SHUKLA R.K., SRIVASTAVA A., SRIVASTAVA A., DUBEY K.C., *J. Cryst. Growth*, 294 (2006), 427.

[11] SARKAR A., GHOSH S., CHAUDHURI S., PAL A.K., *Thin Solid Films*, 204 (1991), 255.

[12] BHOSLE V., TIWARI A., NARAYAN J., *J. Appl. Phys.*, 100 (2006), 033713.

[13] SHARMA B.K., KHARE N., *J. Phys. D Appl. Phys.*, 43 (2010), 465402.

[14] ZHAN Z., ZHANG J., ZHENG Q., PAN D., HUANG J., HUANG F., LIN Z., *Cryst. Growth Des.*, 11 (2011), 21.

[15] LEE J.H., PARK B.O., *Thin Solid Films*, 426 (2003), 94.

[16] OHYAMA M., KOZUKA H., YOKO T., *J. Am. Ceram. Soc.*, 81 (1998), 1622.

[17] YAMAMOTO Y., SAITO K., TAKAKASHI K., KONAGAI M., *Sol. Energ. Mat. Sol. C.*, 65 (2001) 125-132.

[18] SANCHEZ-JUAREZ A., TIBURCIO-SILVER A., ORITZ A., ZIRONI E.P., RICKARDS J., *Thin Solid Films*, 333 (1998), 196.

[19] NATSUME Y., SAKATA H., *Mater. Chem. Phys.*, 78 (2002), 170.

[20] ROY K., ALAM MD.N., MANDAL S.K., DEBNATH S.C., *J. Sol-Gel Sci. Technol.*, 70 (2014), 378.

[21] POLSONGKRAM D., CHAMNINOK P., PUKIRD S., CHOW L., LUPAN O., CHAI G., KHALLAF H., PARK S., SCHULTE A., *J. Phys.-Condens. Mater.*, 403 (2008), 3713.

[22] JUANLIN C., DING C., ZHENHUA C., *J. Sci. China Ser. E*, 52 (2009), 88.

[23] ZHANG X., CHEN Y., ZHANG S., QIU C., *J. Sep. Purif. Technol.*, 172 (2017), 236.

[24] SONG Q., CHEN G., TAN X., TIAN K., *J. Laser Technol*, 38 (2014), 206.

[25] BAGHERI N., MAJLES ARA M.H., GHAZYANI N., *J. Mater. Sci.-Mater.*, 2 (2016), 1293.

[26] MAZILU M., TIGAU N., MUSAT V., *J. Opt. Mater.*, 34 (2012), 1833.

[27] KIM S., KIM M.S., NAM G., LEEM J.-Y., *J. Electron. Mater. Lett.*, 8 (2012), 445.

[28] ZANG J., *M. University of Electronic Science and technology*, 2008, 1.

[29] CHEN K., ZHU H., *J. Chin. Opt. Lett.*, 10 (2015), 256.

[30] VERMA K., CHAUDHARY B., KUMAR V., SHARMA V., KUMAR M., *Vacuum*, 146 (2017), 478.

[31] LIN Y.J., TSAI C.L., LU Y.M., *J. Appl. Phys.*, 99 (2006), 342.

[32] HE Z., XIA Y., TANG B., JIANG X., SU J., *J. Mater. Lett.*, 184 (2016), 148.

[33] LI C., JIN H., YANG Z., *J. Inorg. Mater.*, 02 (2017), 85.

[34] RIDHA N.J., HAFIZUDDIN M., JUMALI H., UMAR A.A., ALOSFUR F., *Int. J. Ectrochem. Sci.*, 8 (2013), 4583.

[35] OPPONG S.O.B., ANKU W.W., SHUKLA S.K., GOVENDER P.P., *J. Res. Chem. Intermed.*, 2 (2016), 2635.

[36] AL-HETLANI E., AMIN M.O., MADKOUR M., *J. Appl. Surf. Sci.*, 411 (2017), 355.

[37] BHATIA S., VERMA N., KUMAR R., *J. Alloy. Compd.*, 726 (2017), 1274.